J. Bangladesh Acad. Sci. 50(2); 181–195: June 2026 DOI: https://doi.org/10.3329/jbas.v50i2.90651

Journal of Bangladesh Academy of Sciences

Journal homepage: http://www.bas.org.bd/publications/jbas.html

Research Article

Environment-friendly anatase TiO_2/cellulose nanocomposites with high surface area for photocatalytic degradation of methylene blue in aqueous system

Enayet Hossain, Md. Sajib, Md. Abu Bin Hasan Susan, and Muhammed Shah Miran*

Department of Chemistry, University of Dhaka, Dhaka 1000, Bangladesh

ARTICLE INFO

Article History

Received: 15 February 2026
Revised: 04 April 2026
Accepted: 10 April 2026

Keywords: Photocatalysis, TiO_2/ Cellulose composite, Wastewater treatment, High surface area.

ABSTRACT

In this study, anatase TiO_2 nanoparticles (NPs) were synthesized via a hydrothermal route from titanium isopropoxide. TiO_2/cellulose nanocomposites were prepared at different weight percentages (20%, 40%, and 60%) and denoted as CT20, CT40, and CT60, respectively, to enhance the photocatalytic degradation of an organic dye. The prepared composites were characterized by FTIR, XRD, FE-SEM, and UV-DRS, confirming the formation of a composite with nano-range particles and a high surface-to-volume ratio. The band gap of the prepared TiO_2 NPs was found to be 3.28 eV. UV radiation was used to investigate the photocatalytic performance of the prepared materials to degrade methylene blue (MB). UV-visible absorption spectroscopy was used to monitor the decrease in MB concentration during photocatalytic experiments. Within 90 min, the removal efficiencies were 83%, 89%, 90%, and 99% for CT20, CT40, CT60, and TiO_2, respectively. The dye removal per mg of TiO_2 in the composite were found to be 8.3%, 4.5%, 3%, and 2%, for CT20, CT40, CT60, and TiO_2, respectively. To investigate the optimum conditions for the photocatalytic degradation reaction, the effects of pH, catalyst dose, and initial dye concentration were studied. The degradation reaction of MB was followed by pseudo-first-order kinetics, with rate constants of 0.010, 0.013, 0.016, and 0.026 min^{-1} for CT20, CT40, CT60, and TiO_2, respectively. Reusability data indicate that composite materials can be recycled across multiple life cycles without compromising cost-effectiveness.

Introduction

Industrialization and urbanization are increasing worldwide as populations grow. Thus, the release of various toxic and persistent pollutants into the environment increases daily. These hazardous compounds from various sources are severely polluting the environment. Water pollution has become a significant concern worldwide. Water is essential for drinking and the survival of aquatic life. The direct disposal of municipal and industrial wastewater into natural pure water sources is the leading cause of water pollution (FN and MF, 2017; O'Shea and Dionysiou, 2012). Therefore, wastewater must be treated before discharging it into waterways. Most synthetic organic pollutants resist natural degradation and thus need to be applied to advanced physicochemical processes (Chalasani and Vasudevan, 2013; Ponomarev and Ershov, 2020; Zhang et al., 2021). Numerous sophisticated methods have been developed in recent years to separate and destroy impurities, including dyes, pharmaceutical

*Corresponding author:<shahmiran@du.ac.bd>

residues, PAHs, insecticides, petrochemicals, and microorganisms. Synthetic dyes and pigments are widely employed in the pharmaceutical, tannery, and textile industries, all producing colored wastewater (Sajib et al., 2025; Giovannetti et al., 2015). During the dying process, especially in textile manufacturing, 10-50% of the dye is lost and discharged into the effluent. The effluent from the colored textile sector contains high concentrations of organic dyes, surfactants, heavy metals, and other hazardous chemicals, posing a serious threat to surface and ground water quality, soil, and aquatic ecosystems (Peternel et al., 2007). Dye concentrations typically range from 10 to 250 ppm. Due to the complex nature of dyes, they are difficult to separate from the aquatic system. The presence of dyes in aquatic environments has several adverse effects, including reduced light penetration and inhibited growth of aquatic organisms due to lowered dissolved oxygen concentrations (Al-Tohamy, et al., 2022). There are several methods for the treatment of wastewater including coagulation, membrane separation, ion exchange, electrochemical, and advanced oxidation processes (AOPs) (Ehsan et al., 2023). AOPs such as ozonation, H_2O_2 treatment, Fenton, photo-Fenton, and semiconductor photocatalysis are more effective and faster in removing persistent organic pollutants from wastewater (Sajib et al., 2026). For the removal of organic pollutants through photocatalysis, the use of TiO_2 has been significantly reported (Al-Mamun et al., 2019; Jallouli et al., 2017; Shohel et al., 2016). TiO_2, a suitable *n*-type semiconductor, can destroy the organic dyes to mineralize into small non-toxic molecules through an electron-hole pair mechanism under UV light (Idris et al., 2022). The aim of this research is to prepare composites of anatase TiO_2 for enhanced dye removal performance. The material used to make a TiO_2 composite will be non-toxic to the environment and biocompatible natural polymer, cellulose. To serve these purposes, cellulose was selected as the supporting material for TiO_2, with the aim of achieving high dye-removal efficiency (Hong, et al., 2023). Aggregation of the nanoparticles and lower adsorption capacity can reduce their photocatalytic performance. Supporting materials, such as cellulose, can enhance the photocatalytic performance of TiO_2 by improving dye adsorption and dispersing the nanoparticles, thereby acting as a matrix material (Hong, et al., 2023). Cellulose is an abundant natural polymer, fully biodegradable, readily available, and inexpensive. It has highly polar groups in its structure and thus has high adsorption capacity.

In this work, anatase TiO_2 NPs were synthesized by the hydrothermal method. TiO_2/cellulose composite materials were prepared to obtain enhanced dye removal performance. The prepared materials were characterized by Fourier transform infrared (FTIR) spectroscopy for functional group analysis, thermogravimetric analysis, X-ray diffraction (XRD) to determine the crystal structure, Field emission scanning electron microscopy (FE-SEM) for morphology analysis, and UV-visible diffuse reflectance spectroscopy (UV DRS) for optical property elucidation. The photocatalytic performance of the prepared materials was evaluated by removing MB from an aqueous solution under UV irradiation. Effect of parameters such as solution pH, catalyst dose, and initial dye concentration was performed to identify the optimal conditions for photocatalysis with these materials. The reusability of the photocatalyst was examined by performing three consecutive photocatalysis runs.

Experimental

Chemicals used

Titanium isopropoxide (TIP) (Sigma-Aldrich, China), 2-propanol (Merck, Germany), *α*-cellulose (Sigma Aldrich, USA), ferric chloride hexahydrate (Loba Chemie, India), ferrous sulfate heptahydrate (Uni-Chem, China), 25% ammonia solution (Merck, India), methylene blue (MB) (Janssen Chimica, Belgium), sodium hydroxide (Merck, Germany), and

hydrochloric acid (Sigma-Aldrich, USA) were used without any further purification. De-ionized water (conductivity: 0.055 μScm^{-1} at 25.0 ℃) from an HPLC-grade water purification system (BOECO, Germany) was used.

Synthesis of nanosized TiO_2

TiO_2 NPs were prepared by a hydrothermal synthesis method. 14.83 mL TIP was added to 100 mL of isopropanol to prepare 4 g TiO_2. The mixture was then sonicated for 15 min to obtain a clear alcoholic solution of TIP. To this solution, 30 mL of isopropanol-water (volume ratio 2:1) mixture was added slowly under constant mechanical stirring for about two hours. A white precipitate was obtained and filtered with Whatman 42 filter paper. This white mass was transferred into a Teflon-lined hydrothermal reactor with a maximum capacity of 80 mL. Water was added to fill about two-thirds of the vessel. This hydrothermal reactor was placed in a muffle furnace and held at 180 °C for 12 h. After cooling to room temperature, the product was collected by filtration and washed several times with DI water. The white residue was then dried overnight at 65 °C. The overall reaction is

$$\mathrm{Ti[OCH(CH_3)_2]_4}(l) + 2\mathrm{H_2O} \rightarrow \mathrm{TiO_2}(s) + 4\mathrm{(CH_3)CHOH}(aq) \quad (1)$$

Preparation of TiO_2/cellulose composites

A specified amount of as-prepared TiO_2 was dispersed in 400 mL of DI water under magnetic stirring and ultrasonication. The specified amount of α-cellulose powder was mixed into the TiO_2 dispersion under vigorous stirring. The dispersion was heated at 60 °C with stirring until complete evaporation. The final material was then dried at 105 °C. Three composites of cellulose and TiO_2, denoted as CT20, CT40, and CT60 were prepared containing 20 wt%, 40 wt%, and 60 wt% TiO_2, respectively. Preparation of TiO_2/cellulose composites is schematically shown in Fig. 1.

Characterization of prepared composites

IR spectra of the CT composites were recorded on a PerkinElmer FTIR spectrometer in transmittance mode over 450-4000 cm^{-1}. KBr was used to make pellets of the samples. XRD patterns of the prepared materials were recorded with a Philips PW 1724 using an XDC-700 Guinier-Hägg focusing camera with strictly monochromatized Cu Kα_1 radiation (λ = 0.154 nm). The powdered samples were placed on two plain glass slides (25nm × 75nm), forming a film, and inserted into the diffractometer. The measurement was performed in continuous mode at a scan rate of 3.0 deg min^{-1} over the 10-90 deg range, with a scan width of 0.026 deg. The optical properties of the prepared samples were investigated from their diffuse reflectance spectra. The reflectance spectra were recorded with a UV-Vis-NIR Spectrophotometer (PerkinElmer, Model: Lambda 1050+, UK). The band gap energies of the composites were determined by using the Kubelka-Munk method. Thermogravimetric analysis (TGA) of TiO_2 and its composites was performed using a Hitachi TG/DTA 7200 in an O_2 atmosphere at a heating rate of 10 °C min^{-1}. The Al pan was used as both a reference and a sample pan. The sensitivity value for TGA was 0.2 μg. UV-vis spectra were recorded using a UV-visible double-beam spectrophotometer (Labomed, UVD-3500) with a wavelength range of 190-900 nm, using a deuterium lamp for the UV source and a tungsten lamp for the visible source. The measurements were carried out in a glass cell over 400-800 nm, with a cell length of 1 cm. DI water was used as the solvent and as a reference for this measurement. The morphology of the prepared composites was studied using FE-SEM (Zeiss, Germany). The acceleration voltage of the electron gun was 5 kV. EDX spectra of the sample were also obtained from the instrument, from which the elemental composition of the composites was deduced.

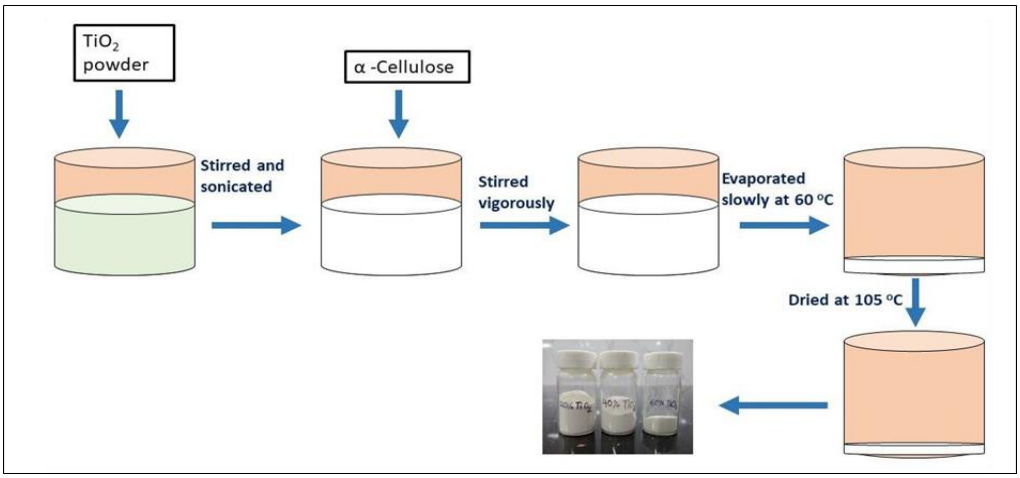

Fig. 1. Preparation of TiO_2/cellulose composites with different weight percentages.

Photocatalytic test

MB was used as a model dye in photodegradation experiments. The experiments were conducted in a 250 mL beaker, using 100 mL of the MB solution at the specified concentrations. The photocatalytic reaction system was inside a cubic box. A 6 W UV-C lamp (Sankyo-Denki, Japan) was mounted on the top of the box as the UV light source, and a magnetic stirrer was placed at the bottom to continuously stir the MB solution during the experiment. The beaker with the MB solution and the catalyst was placed on the magnetic stirrer, and the distance between the lamp and the surface of solution was about 8 cm during the experiments. The photocatalytic experiment started with the addition of the catalyst to the solution. The MB solution with the catalyst was kept in the dark inside the box for 30 min for adsorption-desorption to reach equilibrium. After this period (when equilibrium was established), a small portion of the mixture was transferred from the beaker to a test tube and labeled 0 min. The UV lamp was then immediately switched on. An aliquot of the mixture was withdrawn at 5, 10, 20, 30, 60, and 90 min, and the mixture was centrifuged to separate the catalyst. The absorbance of the solutions was then recorded using a UV-visible spectrophotometer. The absorbance at λ_{max} of MB (664 nm) is directly proportional to the MB concentration and was used to calculate the degradation efficiency. The dye removal percentage was determined by the following formula-

$$\%\ Removal\ of\ Dye = \frac{C_0 - C_t}{C_0} \times 100 \qquad (2)$$

where C_0 is the initial dye concentration, and C_t is the concentration after a certain time, t.

Results and Discussion

Molecular characterization by FTIR spectroscopy

Molecular properties of the CT composites, TiO_2, and cellulose was investigated by FTIR spectroscopy. The FTIR spectra of these materials are shown in Fig. 2. α-cellulose shows a strong and broad absorption near 3440 cm^{-1} due to the stretching of O-H groups in its structure (Poletto et al., 2011). The broadband near 3400 cm^{-1} in the spectrum of TiO_2 is due to the O-H stretching vibration of the adsorbed water on its surface. Nanocrystalline materials have a high surface-to-volume ratio, thus strongly adsorb moisture from the atmosphere. The bands at 1431, 1375, 1336, and 1318 cm^{-1} are associated with CH_2, in-plane CH deformation, in-plane OH bending, and CH_2 wagging, respectively. The bands at 1164, 1112, 1058, 1027, 896, and 670 cm^{-1} are attributed to the asymmetric C-O-C bridge stretching, the anhydro-glucose ring, C-O-R stretching, C-O-C pyranose ring skeletal vibration, CH deformation, and out-of-plane OH bending, respectively (Poletto et al., 2011). The broad peak near 600 in the TiO_2 spectrum corresponds to the Ti-O-Ti bending vibration. The presence of both cellulose and TiO_2 bands in the spectra of the composites indicates the successful incorporation of TiO_2 in the cellulosic structure.

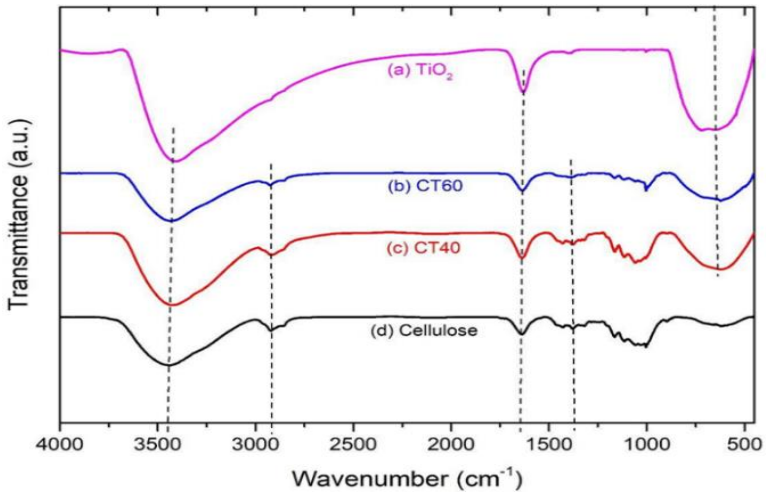

Fig. 2. FT-IR spectra of the composites, TiO_2, and cellulose powder.

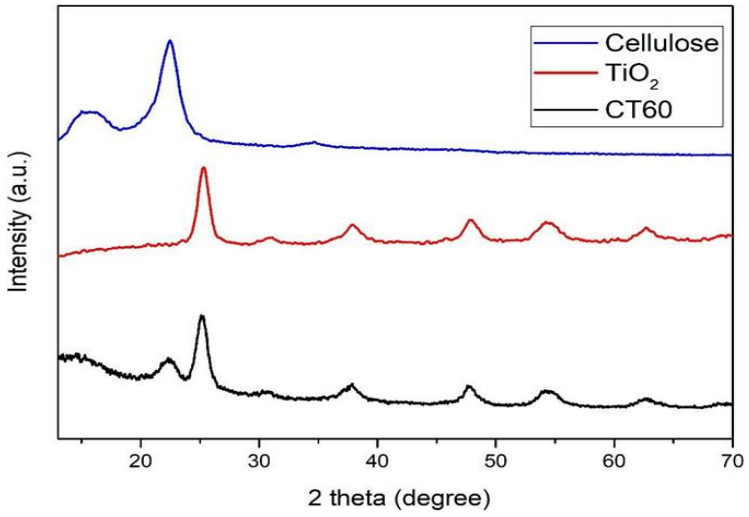

Fig. 3. XRD patterns of cellulose, TiO_2, and CT60.

Analysis of crystal structure by XRD

XRD pattern of cellulose, TiO_2, and their composite CT60 are shown in Fig. 3. Cellulose has an intense peak at 14.2° and 22.4°, which corresponds to the crystal plane (110) and (002), respectively. A weak peak at 34.6° corresponds to the (004) plane. In the XRD pattern of TiO_2, prominent peaks characteristic of the anatase structure are observed, which matched with the previously recorded XRD patterns of anatase TiO_2 (ICDD card no: #00-021-1272) (Ullah et al., 2026). The peaks located at 25.3°, 37.9°, 48.1°, 54.0°, 55.1°, and 62.7° correspond to the characteristic planes of anatase (101), (004), (200), (105), (211), (204), respectively (Muniandy et al., 2017). Anatase TiO_2 was successfully synthesized by the hydrothermal method. Among the crystal forms of TiO_2, anatase is the most efficient as a photocatalyst (Luttrell et al., 2014). In the pattern of CT60, all the corresponding peaks of TiO_2, along with the cellulose peak was present. It confirms the successful synthesis of CT composites in this work. The composites are expected to exhibit good photocatalytic activity owing to the presence of anatase TiO_2.

Morphology analysis by FE-SEM

The morphology of the prepared materials was investigated by FE-SEM analysis. It reveals the size and shape of the prepared materials. The FE-SEM images of TiO_2, α-cellulose, and TiO_2-cellulose (CT60) composite are shown in Fig. 4.

The particle shape of the α-cellulose was found to be micro fibrous, with an approximate diameter of 25 µm. It is clear from the FE-SEM image that spherical-shaped nanoparticles of TiO_2 were obtained using hydrothermal synthesis from TIP. The average diameter of the particles of TiO_2 was found to be 35 nm. In the FE-SEM images of CT60 composite (Fig. 4), it is clear that the nano TiO_2 were dispersed in the surface of the cellulose microfibers. This dispersion leads to the reduction of the aggregation behavior and exposed the hidden surface area covered in the aggregated form, leading to enhancement of the surface-to-volume ratio of the materials. The material has a high surface-to-volume ratio and is expected to exhibit high chemical activity. The photocatalytic performance of the materials was proportionally dependent on the size and surface-to-volume ratio of the photocatalyst particles. Lower particles show high photocatalytic performance due to their high surface-to-volume ratio. These nanosized particles exhibit increased light absorption and a greater surface area for adsorbing water and dissolved oxygen, which subsequently generate reactive oxygen species (ROS) via photocatalysis. Higher ROS production leads to greater dye degradation efficiency.

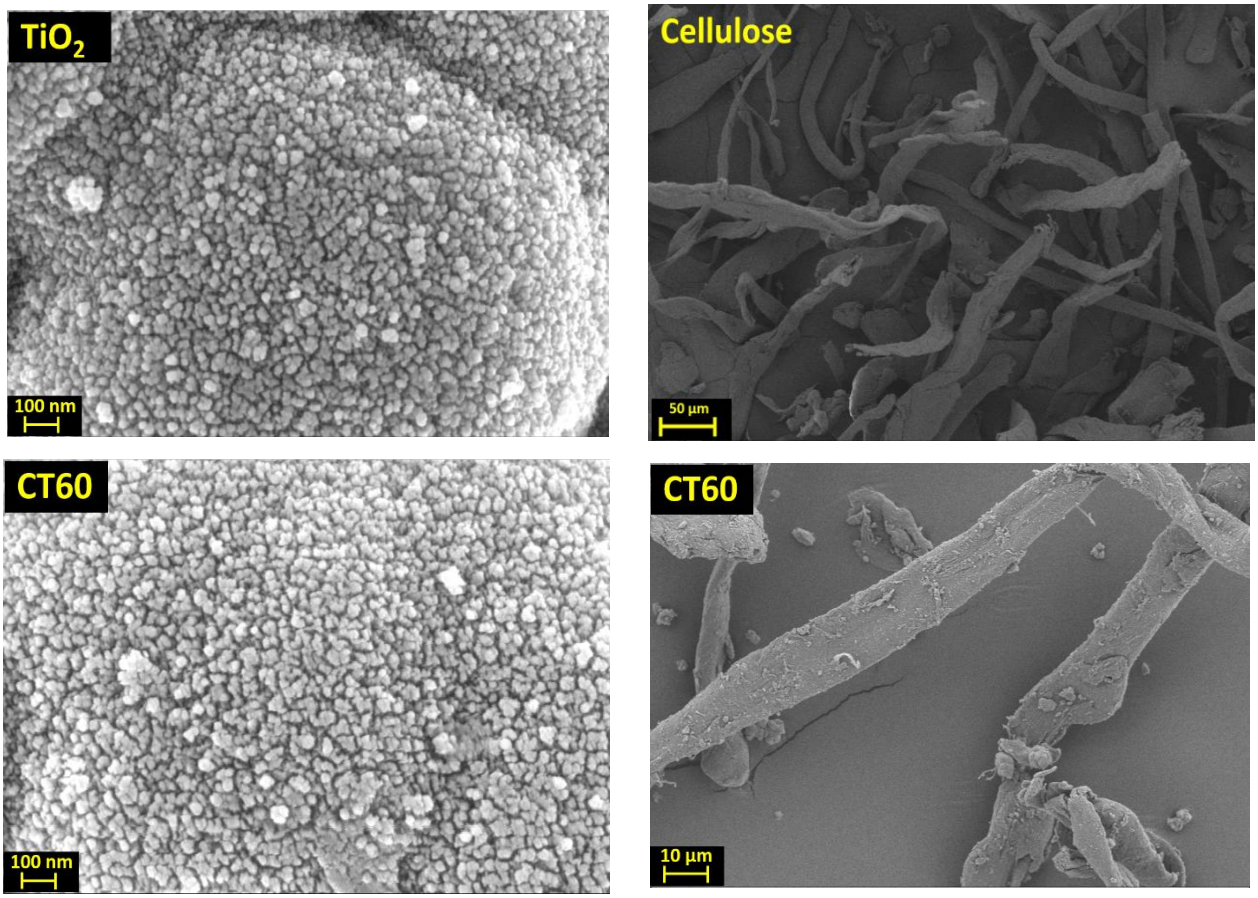

Fig. 4. FE-SEM images of TiO_2, α-cellulose, and TiO_2-cellulose (CT60) composite.

Elemental analysis by EDX Spectroscopy

The elemental analysis of the prepared materials were investigated by the data from energy dispersive X-ray (EDX) spectroscopy. The EDX spectra of TiO_2, cellulose, and CT60 composite were shown in Fig. 5. There were peaks found for the responsible for Ti and O in the spectrum of TiO_2, indicating the successful preparation of the materials. Similarly, there were peaks responsibe for C and O in the spectrum of cellulose. These peaks (Ti, O, and C) were also found in the spectrum of CT60 composite in their respective position, indicating the successful preparation of the composite of TiO_2-Cellulose.

The quantitative analysis of the elements present in CT60 were carried out and the data of the wight and atomic percentages of Ti, C, and O were given in Table 1. From that, the weight percentage of Ti present in the CT60 composite was found to be 22 %, while the weight percentage of C and O were found to be 31 and 47%, respectively.

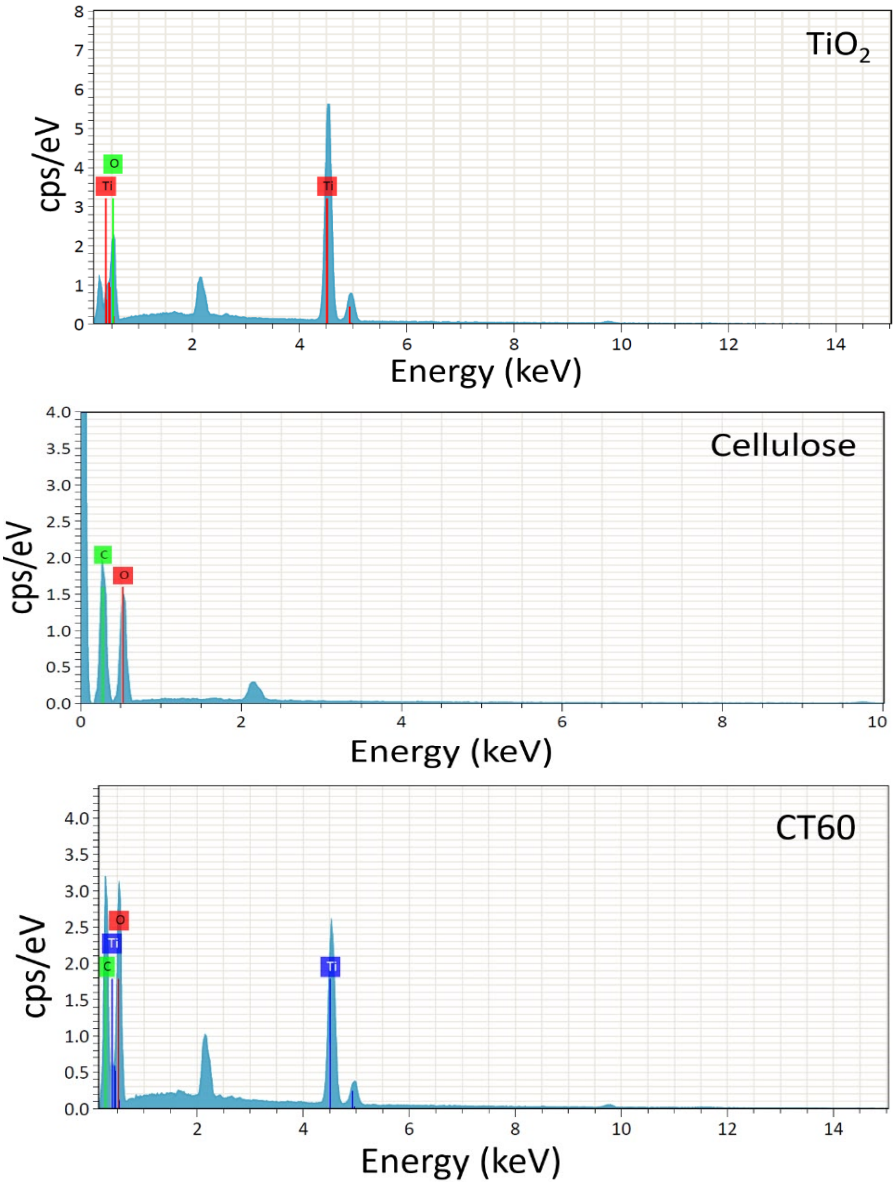

Fig. 5. EDX spectra of TiO_2, cellulose, and CT60 composite.

Table 1. Weight and atomic percentages of Ti, C, and O in CT60 composite.

Materials	Elements	Weight percentage (%)	Atomic percentage (%)
CT60	Ti	22	8
	C	31	43
	O	47	49

Optical Properties by UV DRS

Optical properties of the prepared materials were investigated by UV-vis DRS. Tauc plots of CT40, CT60, and TiO_2 were obtained by the Kubelka-Munk method, as shown in Fig. 6. The band gap energies (E_g) of the materials were calculated. The value of E_g for TiO_2 was found to be 3.28 eV, which matched the band gap energy of anatase TiO_2. This is also a clear indication of the successful synthesis of anatase TiO_2 through a facile hydrothermal method. The composites both CT60 and CT40 have the same E_g value with TiO_2 NPs. It happens because the cellulose fibers do not distort the TiO_2 structure. TiO_2 NPs merely have some physical interactions with the surface of fibers and the tendency of agglomeration is reduced.

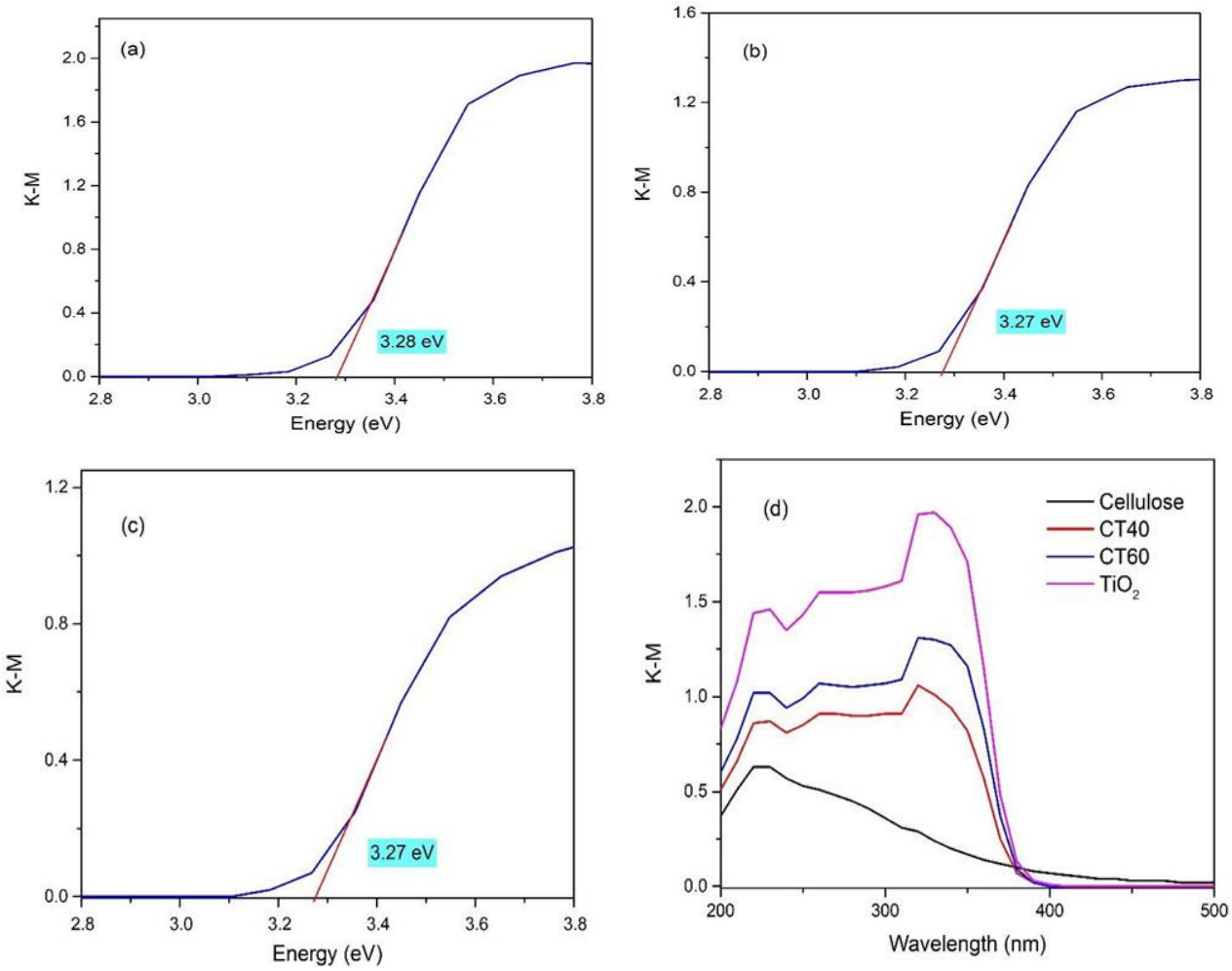

Fig. 6. Tauc plots of a) TiO_2, b) CT60, and c) CT40; d) the Kubelka-Munk function versus wavelength.

Photocatalytic degradation of MB dye optimization of the reaction parameters

Effect of pH

pH of the solution significantly affects photocatalysis. Due to the surface charge of the particles dispersed into solution depends on the pH value. The surface properties of the TiO_2 NPs attached to the cellulose fibers have a significant impact on photocatalytic activity. The zeta potential and the consequences related to it are determined by the pH of the solution. Thus, pH has a crucial rule on photocatalysis mechanism (Hayati et al., 2018). The pH dependency of the photocatalytic performance of the composite CT60 is shown in Fig. 7 (a). It is clear that higher dye removal efficiency was obtained at an alkaline pH of the dye solution. The dye-removal efficiency of the photocatalyst decreases significantly as the pH of the MB solution decreases. A basic pH of the solution results in better dye-removal performance. The poor dye removal efficiency at acidic pH is due to changes in the surface properties NPs with solution pH. The surface of TiO_2 is inherently negative, i.e., it possesses a negative zeta potential value. In acidic pH, the negative charge of the surface is neutralized by H^+ ions, present in excess in the solution (Binazadeh et al., 2023). Therefore, the adsorption of MB is lower at acidic pH onto the surface of TiO_2. Dye degradation also decreases because adsorption plays a vital role in the photodegradation process. In alkaline conditions, on the contrary, the negative charge of the surface remains higher, and adsorption of the cationic MB dye occurs efficiently. Also, the presence of higher OH^- ions in the solution accelerates the formation of $OH^•$ radicals. The formation of $OH^•$ radicals has an enormous effect on the degradation and mineralization of organic compounds. The dye removal efficiency increases with pH up to pH = 8, after which it remains nearly constant at pH = 10. The pH of the prepared MB solution was 8, and maximum efficiency was observed at this pH.

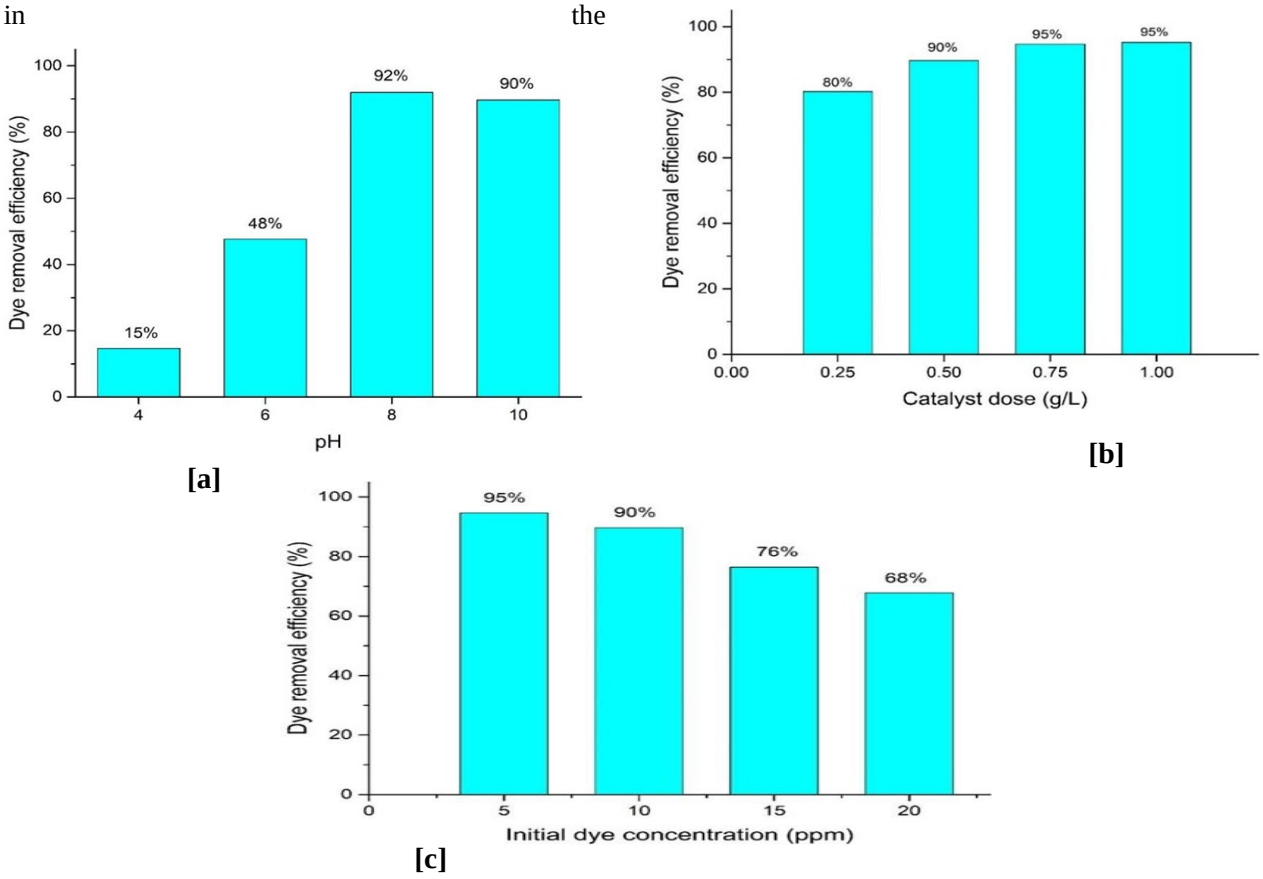

Fig. 7. Effect of a) pH, b) catalyst dose, and c) initial dye concentration on photocatalytic reaction.

Effect of catalyst dose

The amount of catalyst in the solution during the photocatalytic process plays an essential role in the photodegradation of organic pollutants. The total surface area of the photocatalyst increases with an increase in the dosage of the photocatalyst. A larger surface area means there are more active sites on the catalyst surface, thereby enhancing the reaction rate. In heterogeneous catalysis, the extent of reaction is directly related to the surface area of the solid catalyst (Saravanan et al., 2017). The effect of CT60 photocatalyst dosage was investigated by varying the amount of catalyst. The experiments were conducted at catalyst dosages of 0.25 to 1 g L^{-1}, initial pH of 8, dye concentration of 10 ppm, and irradiation time of 90 min. The change in degradation efficiency of the CT60 catalyst with different catalyst dosages is shown in Fig. 7(b). With the photocatalyst dosage increasing from 0.25 to 0.75 g L^{-1}, the specific surface area increased, resulting in a greater number of active sites and enhanced MB degradation from 80% to 95%. However, when the catalyst concentration exceeds 0.75 g L^{-1}, MB degradation does not change. The literature indicates that, beyond the optimal photocatalyst dosage, the degradation rate decreases rather than increases with excess catalyst in solution (Elhalil et al., 2018). The reasons behind this may be: (I) increased opacity of solution, light scattering, results in the prevention of light from entering into the solution depth; (II) aggregation of particles which diminishes available surface area of the catalyst.

Effect of initial dye concentration

Generlly, the photodegradation performance is the highest when the initial substrate concentration is kept at a low (Babu et al., 2019). The effect of dye concentration was examined at different concentrations of 5–20 ppm, initial pH of 10, catalyst dosage of 0.5 g L^{-1}, and irradiation time of 90 min. Fig. 7(c). shows the result of the change in degradation efficiency with varying dye concentration. The degradation efficiency is 68% at a concentration of 20 ppm. Efficiency increases significantly as the phenol concentration decreases from 20 to 5 ppm. At higher dye concentrations, a large portion of irradiated light is absorbed by dye molecules and their intermediate by-products. This decreases the exposure of photocatalyst to the light photon and thus lowers the concentration $^{\bullet}OH$ radicals (Hayati et al., 2018). As a result, the photocatalytic activity is reduced in high concentrations of dye. Also, it can be inferred that the elevation of dye concentration and its intermediate by-products deactivate the reaction sites and reduce the light penetration to reach the active sites of the catalyst surface, which are accountable to produce reactive radicals.

Removal of MB using CT composites

The photocatalytic activity of the prepared materials, including pure TiO_2 and its composites with cellulose was evaluated by using MB as a model dye and UV light as a radiation source. Before UV irradiation, the catalyst-mixed solution was kept in the dark for 30 min under constant stirring. Approximately 33% of the dye was adsorbed on the catalyst surface. After that, UV irradiation was continued for 90 min to observe the extent of removal of MB through photocatalysis. Absorption spectra for the removal of MB by CT60 are shown in Fig. 8. The absorption peak of MB gradually decreased over time, and after 90 min, the dye was completely removed from the solution. This is an excellent result compared with other work in the literature. In all experiments, the dye solution was stirred with the catalyst in dark conditions for 30 min to reach the adsorption-desorption equilibrium. In the case of cellulose, dye adsorption occurs only.

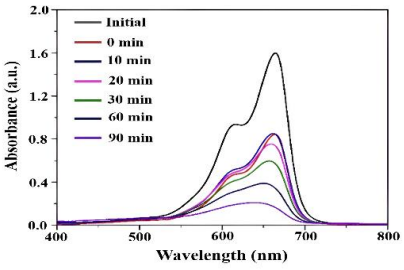

[a]

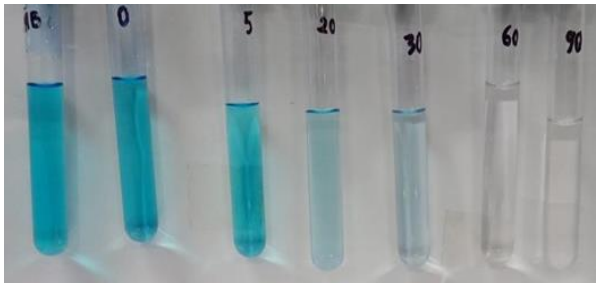

[b]

Fig. 8. a) Photocatalytic removal of MB by CT60 and b) color change of the MB dye during photocatalytic degradation (Initial dye concentration: 10 ppm, catalyst dose: 0.5 g L^{-1}, and pH: 8).

Kinetic study of the photocatalytic reaction

The dynamic plot for the removal of MB using different photocatalysts are shown in Fig. 9. A blank run was performed without any catalyst under UV light irradiation. No significant change in the concentration of MB was observed. Initially, the dye removal occurred via adsorption on the catalyst surface. Cellulose has a high adsorption capacity due its polar surface. The TiO_2 NPs exhibit the lowest adsorption among the materials. The adsorption of CT40 is higher than that of CT60, but the final dye removal is similar to that of CT60. The reason may be adsorption and degradation of MB on the TiO_2 surface. Approximately 90% of MB was removed within 90 min using these two composites. CT20 has a dye-removal efficiency of 83%, which is notable as well. So, it is clear that with cellulose as a supporting material, TiO_2 can remove dye from the solution with a lower amount of TiO_2. Thus, the treatment of wastewater can be possible by using a low amount of TiO_2, which reduces the cost of material and also pollution due to nanoparticle exposure into the environment, and also decreases. The major advantage of using cellulose with TiO_2 is the ease of separating solid materials after the treatment process. This will enhance photocatalyst recovery and enable reuse for several cycles. Fig. 9. illustrates the degradation rate and reaction kinetics of photodegradation of MB with different photocatalysts. The pseudo-first-order rate constants (k) for the photocatalytic reaction of MB were calculated from the slope of the linear plot of $-\ln(C_t/C_0)$ vs time. The rate constant of the reaction was obtained using the Langmuir–Hinshelwood model, which is commonly applied to photocatalytic degradation processes when the initial pollutant concentration is low (Moniz et al., 2014). The linear equation for the pseudo first-order reaction is given as-

$$\ln\left(\frac{C_0}{C_t}\right) = k\mathrm{t} \qquad (3)$$

where C_0 and C_t are the concentrations of aqueous solution of MB at 0 and t min, respectively.

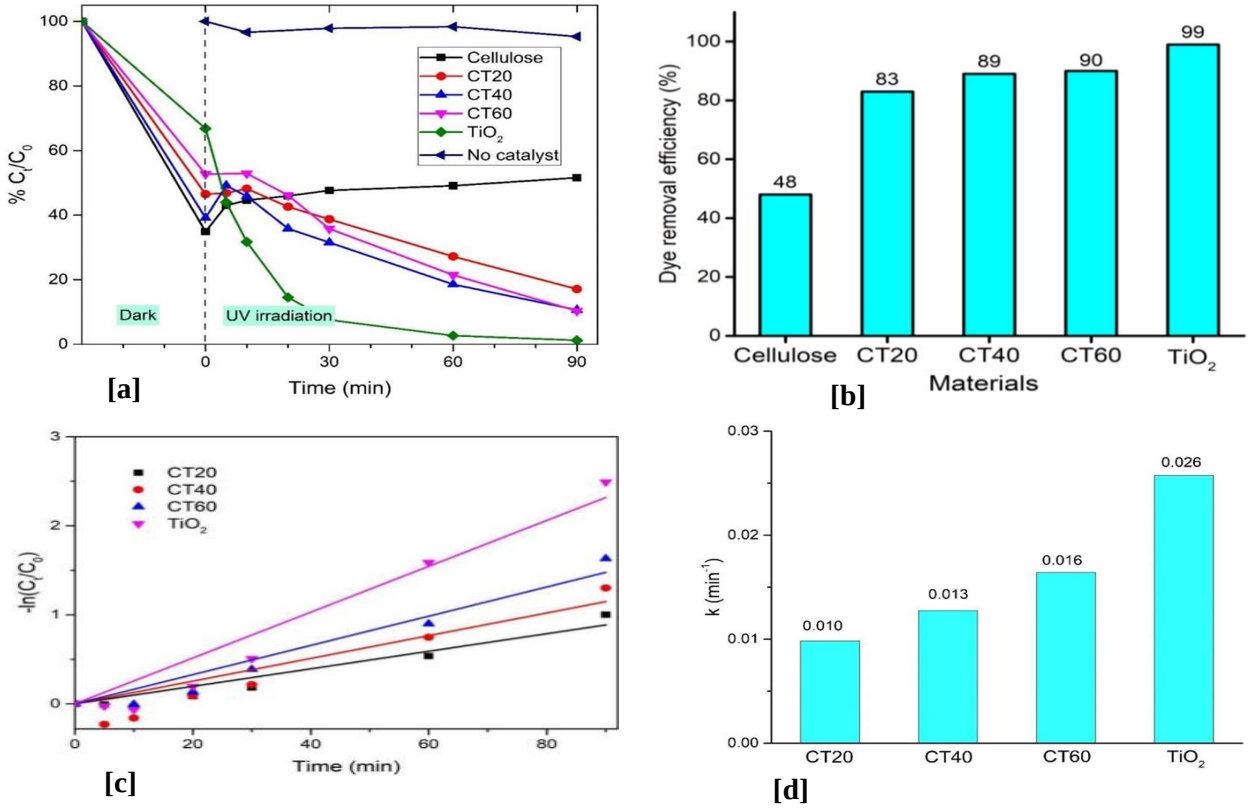

Fig. 9. a) Dynamic plot, b) bar plot of the removal of MB, c) kinetic plot, and d) pseudo first order rate constant of the photocatalytic degradation reaction of MB (Initial MB concentration: 10 ppm, catalyst dose: 0.5 g L^{-1}, and pH: 10).

It is evident that TiO_2 NPs show the fastest kinetics among the photocatalysts (Fig. 9). The prepared TiO_2 NPs have a surface area due to their small size. Therefore, TiO_2 NPs show excellent photocatalytic performance. As the wt% of cellulose in the composites increases, the dye removal efficiency decreases because the amount of TiO_2, the main photocatalyst, decreases. The main purpose of incorporating cellulose is to make the catalyst separation process easier. Cellulose also facilitates the photodegradation of TiO_2 by adsorbing dye molecules, bringing them closer to the catalyst surface. The comparison of *k* of the photocatalysts is depicted in Fig. 9. Although the highest dye removal was achieved with pure TiO_2 NPs, the dye removal obtained with the CT composites is better than that with pure TiO_2, even at lower TiO_2 loadings. The composites exhibit excellent dye-removal efficiency at lower TiO_2 contents. The dye removal efficiency per mg of TiO_2 present in the composites is given in Fig. 10.

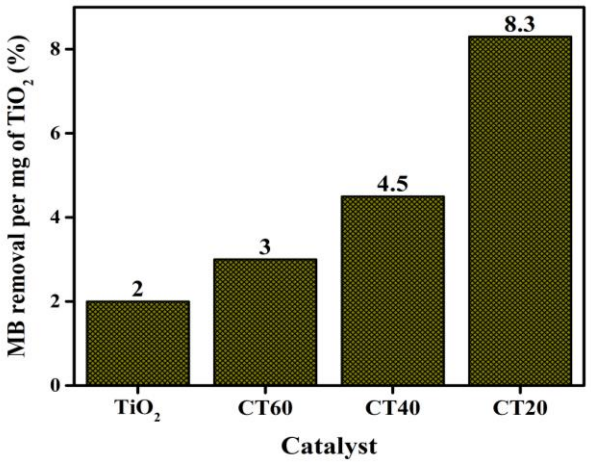

Fig. 10. Percentage of MB removal per mg of TiO_2 by the prepared catalysts.

In each dye removal experiment, 50 mg of catalyst was mixed with 100 mL of the MB solution. The dye removal per mg of TiO_2 in the composite were found to be 8.3%, 4.5%, 3%, and 2%, for CT20, CT40, CT60, and TiO_2, respectively. It might be due to the high surface area of active photocatalyst since TiO_2 was embedded on the surface of the cellulose compared to pure catalyst.

Reusability of the photocatalyst

The recyclability of CT60 was investigated by conducting 3 photocatalysis runs using the recycled catalyst. The experiments were carried out under previously optimized conditions such as, catalyst dose was used 0.5 g L^{-1} in the pH of 10 for 60 min UV irradiation, and initial dye concentration used 10 ppm. After every experiment, the used catalyst was washed with ethanol several times to remove adsorbed unreacted MB on the surface of the catalyst, centrifuged, and dried in an oven at 60 °C overnight. Fig. 11 shows the recyclability of the prepared CT60 materials. The dye removal efficiency remained above 85% after three cycles, indicate that CT60 has a good stability and recyclability in dye-removal performance. The reduction in photocatalytic activity from 95% to 85% after three consecutive cycles can be attributed to leaching of TiO_2 from the composite in the washing process. Another reason may be the presence of previously adsorbed dye and its by-products, which covered the active sites of the catalyst. The adsorption capability of the photocatalyst may decline due to a reduction in the surface area of the photocatalyst due to aggregation in aqueous solution.

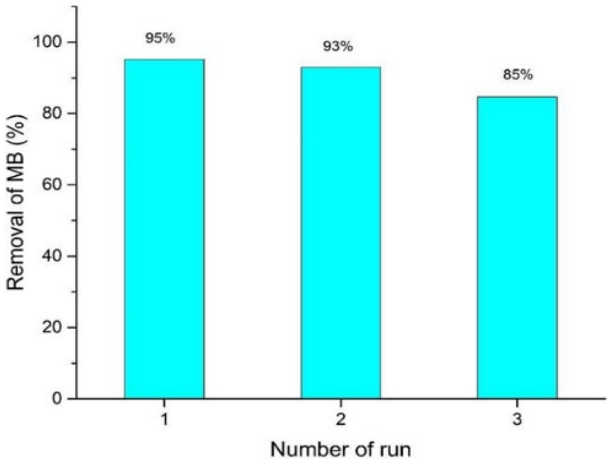

Fig. 11. The reusability of the CT60 photocatalyst for three runs.

Possible photocatalytic mechanism

The possible reaction mechanism of heterogeneous photocatalysis is illustrated in Fig. 12.

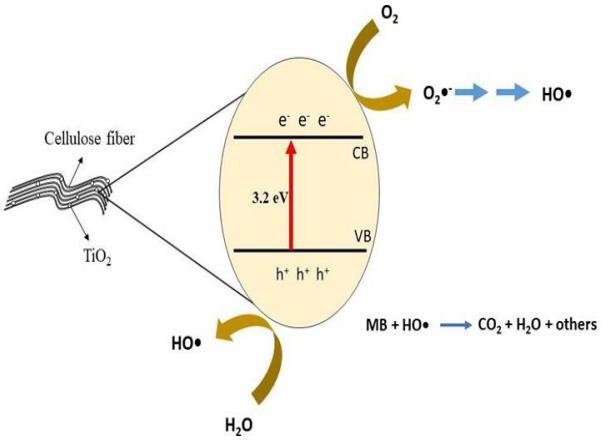

Fig. 12. Proposed mechanism of photodegradation of MB with TiO_2/cellulose composites.

The mechanism of photocatalysis with semiconductors has been established in many literatures. The photodegradation process begins with the excitation of TiO_2 NPs that adhere to the surface of cellulose fibers. Electrons from the valence band of TiO_2 jump into the conduction band by irradiation of UV radiation, leaving behind a hole in the valence band. After each event of excitation, an electron-hole pair results in the valence band becoming a positive hole-dominant region and the conduction band rich in negative electrons.

Conclusion

Anatase TiO_2/cellulose/ composites were prepared, which are easily separable from solution after water treatment because TiO_2 NPs were immobilized on the cellulose surface. The CT composites show excellent photocatalytic activity under UV light due to the embedded photocatalyst over the surface of cellulose in the composite. By optimizing reaction parameters, including solution pH, catalyst dose, and initial dye concentration, the optimal conditions for dye removal were established. The highest dye removal was achieved at an ambient pH of 8 for a 10 ppm MB solution. About 99% of the dye was removed by TiO_2 within 90 min. It appears that the highest dye removal occurs with TiO_2. Regarding TiO_2 loadings in the composite, CT40 and CT60 are the best photocatalysts at 40 and 60 wt% TiO_2, respectively, achieving 90% MB removal. The CT60 photocatalyst shows excellent recyclability, as the loss of TiO_2 NPs was minimized after incorporation with cellulose fibers, and the tendency for TiO_2 NPs aggregation in aqueous solution also decreased.

Acknowledgment

The authors acknowledge support from the University of Dhaka, Dhaka, Bangladesh.

Authors contribution

Enayet Hossain: Methodology, Investigation, Visualization, Formal Analysis, Writing-original draft; Md. Sajib: Investigation, Methodology, Formal analysis, Writing - Original draft; Md. Abu Bin Hasan Susan: Resources, Review and Editing; Muhammed Shah Miran: Conceptualization, Resources, Writing – review and Editing, Funding acquisition, Visualization, Supervision.

Conflict of interest

There are no conflicts to declare.

Data availability

Data will be made available on request.

References

Al-Mamun MR, Kader S, Islam MS, and Khan MZH. Photocatalytic activity improvement and application of UV-TiO_2 photocatalysis in textile wastewater treatment: A review. *J. Environ. Chem. Eng.* 2019; 7(5): 103248.

Al-Tohamy R, Ali SS, Li F, Okasha KM, Mahmoud YAG, Elsamahy T, and Sun J. A critical review on the treatment of dye-containing wastewater: Ecotoxicological an,d health concerns of textile dyes and possible remediation approaches for environmental safety. *Ecotoxicol. Environ. Saf.* 2022; 231: 113160.

Babu SG, Karthik P, John MC, Lakhera SK, Ashokkumar M, Khim J, and Neppolian B. Synergistic effect of sono-photocatalytic process for the degradation of organic pollutants using CuO-TiO_2/rGO. *Ultrason. Sonochem.* 2019; 50: 218-223.

Binazadeh M, Rasouli J, Sabbaghi S, Mousavi SM, Hashemi SA, and Lai CW. An overview of

photocatalytic membrane degradation development. *Mater.* 2023; 16(9): 3526.

Chalasani R and Vasudevan S. Cyclodextrin-functionalized Fe_3O_4@TiO_2: Reusable, magnetic nanoparticles for photocatalytic degradation of endocrine-disrupting chemicals in water supplies. *ACS Nano*, 2013; 7(5): 4093–4104.

Ehsan MF, Barai HR, Islam MM, Susan MABH, Joo SW, and Miran MS. ZnO nanocomposites supported by acid-activated kaolinite as photocatalysts for the enhanced photodegradation of an organic dye. *Mater. Today Commun.*, 2023; 36: 106563.

Elhalil A, Elmoubarki R, Farnane M, Machrouhi A, Sadiq M, Mahjoubi FZ, Qourzal S, and Barka N. Photocatalytic degradation of caffeine as a model pharmaceutical pollutant on Mg doped ZnO-Al_2O_3 heterostructure. *Environ. Nanotechnol. Monit. Manage.* 2018; 10: 63–72.

FN C and MF M. Factors affecting water pollution: A review. *J. Ecosys. Ecograph.* 2017; 07(01): 1000225

Giovannetti R, Amato CAD, Zannotti M, Rommozzi E, Gunnella R, Minicucci M, and Di Cicco A. Visible light photoactivity of polypropylene coated nano-TiO_2 for dyes degradation in water. *Sci. Rep*. 2015; 5(1): 17801.

Hayati F, Isari AA, Fattahi M, Anvaripour B, and Jorfi S. Photocatalytic decontamination of phenol and petrochemical wastewater through ZnO/TiO_2 decorated on reduced graphene oxide nanocomposite: influential operating factors, mechanism, and electrical energy consumption. *RSC Adv*. 2018; 8(70): 40035–40053.

Hong Y, Islam SR, Liang G, Tang X, She X, and Jiang J. A novel structure of cellulose-TiO_2 nanocomposite for ultra-fast and recyclable organic dyes degradation in wastewater. *J. Environ. Chem. Eng.* 2023; 11(6): 111236.

Idris NHM, Cheong KY, Kennedy BJ, Ohno T, and Lee HL. Buoyant titanium dioxide (TiO_2) as high performance photocatalyst and peroxide activator: A critical review on fabrication, mechanism and application. *J. Environ. Chem. Eng.*, 2022; 10(3): 107549.

Jallouli N, Elghniji K, Trabelsi H, and Ksibi M. Photocatalytic degradation of paracetamol on TiO_2 nanoparticles and TiO_2/cellulosic fiber under UV and sunlight irradiation. *Arab. J. Chem.* 2017; 10: S3640–S3645.

Luttrell T, Halpegamage S, Tao J, Kramer A, Sutter E, and Batzill M. Why is anatase a better photocatalyst than rutile? - Model studies on epitaxial TiO_2 films. *Sci. Rep.* 2014; 4(1): 4043.

Moniz SJA, Shevlin SA, An X, Guo Z, and Tang J. Fe_2O_3–TiO_2 nanocomposites for enhanced charge separation and photocatalytic activity. *Chem. Eur. J.* 2014; 20(47): 15571–15579.

O'Shea KE and Dionysiou DD. Advanced Oxidation Processes for Water Treatment. *J. Phys. Chem. Lett.* 2012; 3(15): 2112–2113.

Peternel IT, Koprivanac N, Božić AML, and Kušić HM. Comparative study of UV/TiO_2, UV/ZnO and photo-fenton processes for the organic reactive dye degradation in aqueous solution. *J. Hazard. Mater*. 2007; 148(1-2): 477–484.

Poletto M, Pistor V, Zeni M, and Zattera AJ. Crystalline properties and decomposition kinetics of cellulose fibers in wood pulp obtained by two pulping processes. *Polym. Degrad. Stab.* 2011; 96(4): 679–685.

Ponomarev AV and Ershov BG. The Green Method in Water Management: Electron Beam Treatment. *Environ. Sci. and Technol.*, 2020; 54(9): 5331–5344.

Muniandy S, Mohd Kaus NH, Jiang Z-T, Altarawneh M, and Lee HL. Green synthesis of mesoporous anatase TiO_2 nanoparticles and their photocatalytic activities. *RSC Adv*. 2017; 7(76): 48083–48094.

Sajib M, Jaman A, Ullah MA, Susan MABH, and Miran MS. AI Technologies for treating petroleum wastewater. In: *management of petroleum wastewater and oil field discharges:*

Diagnosis, Impacts and Treatment. Cham: Springer Nature Switzerland, 2025; 81−118.

Sajib M, Ehsan F, Jaman A, Islam MM, Susan MABH, and Miran MS. Lotus-shaped CuO/ZnO nanocomposites with tunable band gap for UVA-induced photocatalytic degradation of organic dyes. *ACS Omega,* 2026; 11: 19258−19270.

Saravanan R, Gracia F, and Stephen A. *Basic Principles, Mechanism, and Challenges of Photocatalysis,* 2017; pp. 19−40.

Shohel M, Miran MS, Susan MABH, and Mollah MAY. Calcination temperature-dependent morphology of photocatalytic ZnO nanoparticles prepared by an electrochemical–thermal method. *Res. Chem. Intermed.* 2016; 42: 5281-5297.

Ullah MA, Robel FN, Bahadur NM, Islam D, Ahmed S, and Hossain MS. Exploring facet-engineered anatase nanoparticles for amplification of sensitivity in heavy metal ion detection and other applications. *Mater. Adv.* 2026; 7: 1233−1249.

Zhang G, Ruan J, and Du T. Recent advances on photocatalytic and electrochemical oxidation for ammonia treatment from water/wastewater. *ACS ES and T Eng.* 2021; 1(3): 310−325.